

SAC-Loco: Safe and Adjustable Compliant Quadrupedal Locomotion

Aoqian Zhang¹, Zixuan Zhuang², Chunzheng Wang¹, Shuzhi Sam Ge¹, Fan Shi¹ and Cheng Xiang¹

Abstract—Quadruped robots are designed to achieve agile locomotion by mimicking legged animals. However, existing control methods for quadrupeds often lack one of the key capabilities observed in animals: adaptive and adjustable compliance in response to external disturbances. Most locomotion controllers do not provide tunable compliance and tend to fail under large perturbations. In this work, we propose a switched-policy framework for compliant and safe quadruped locomotion. First, we train a force-compliant policy with adjustable compliance levels using a teacher-student reinforcement learning framework, eliminating the need for explicit force sensing. Next, we develop a safe policy based on the capture point concept to stabilize the robot when the compliant policy fails. Finally, we introduce a recoverability network that predicts the likelihood of failure and switches between the compliant and safe policies. Together, this framework enables quadruped robots to achieve both force compliance and robust safety when subjected to severe external disturbances.

I. INTRODUCTION

Compliance is a fundamental principle of locomotion observed in both humans and animals. When subjected to external forces, legged animals exhibit versatile responses: they may resist disturbances or comply to them. Under strong perturbations, animals instinctively move in the direction of the applied force to maintain balance and avoid falling. Achieving similar compliant behaviors in legged robots is crucial for safety and stability. Moreover, compliance extends beyond self-protection, it could further enhance adaptive locomotion in unstructured environments, facilitates safer physical interaction with humans, and supports cooperative tasks such as collaborative object transport.

Reinforcement learning (RL) controllers have been shown to be highly effective in allowing quadruped robots to perform a wide range of tasks, such as complex terrain traversal [1], physical interaction with objects [2], [3], and obstacle avoidance [4]. While RL-based controllers can achieve whole-body control, robust and adaptive response to external forces remain a significant challenge. Most existing approaches emphasize strict task execution, such as tracking velocity or position regulation [5], [6], while neglecting the effects of persistent external disturbances. Although deep RL inherently provides some robustness to perturbations, achieving versatile responses across a broader range of external forces requires more sophisticated learning strategies. To this end, both model-based approaches [7] and learning-based methods [8] have been explored for disturbance compliance. However, these methods often produce limited behavioral

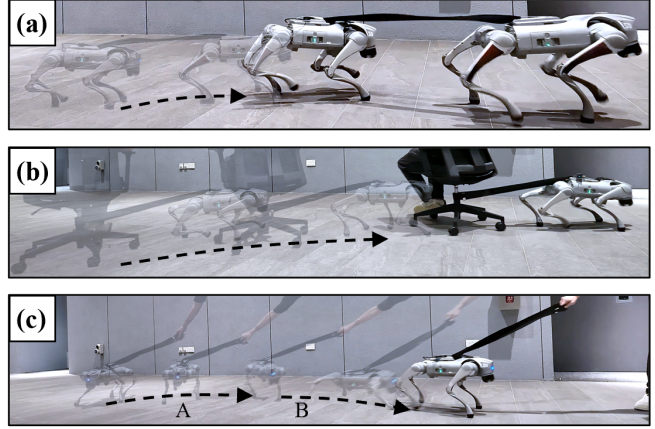


Fig. 1. (a). A quadruped robot pulling the compliant follower robot. (b). Quadruped robot pulling a human on a chair. (c). A: Quadruped robot executing the compliant policy and move along with a pulling force and B: jump toward the pulling force to restore balance using the safe policy

diversity, leading to failures when facing large or prolonged disturbances. This highlights the need for a controller that, like legged animals, can flexibly decide whether to resist, yield, or move with the force to maintain balance and accomplish tasks safely.

To address this challenge, we propose SAC-Loco, a safe and adjustable compliant switched policy control framework that consists of a velocity-based force compliant control and a safe policy for failure prevention. A policy switching mechanism is proposed to detect potential failure and switch between the compliant policy and the safe policy. The main contributions of this work are as follows:

- An end-to-end joint-level locomotion policy with adjustable compliance, enabling adaptive motion under external forces while ensuring velocity tracking and robustness against large disturbances.
- A lightweight distillation framework that enables on-board deployment without an additional force estimation module, while allowing the student policy to match the performance of the teacher policy.
- A recoverability network that conditions on compliant and safe policies to determine switching timing, ensuring smooth compliance under safe interactions and reliable recovery under large disturbances.
- Extensive simulations and hardware experiments validate the effectiveness of the proposed method.

II. RELATED WORKS

For external force-compliant and safe control of legged robots, some existing work adopts model-based methods to

¹Department of Electrical and Computer Engineering, National University of Singapore.

²School of Computer Science and Engineering, Sun Yat-sen University.

estimate the external forces acting on the robot. Khandelwal et al. proposed a method using only proprioceptive feedback to estimate the external forces [9], which has been shown to provide force estimations that can be directly leveraged by an admittance controller for payload transportation. Beyond using proprioceptive information, Kang et al. proposed multimodal sensing by combining IMU and vision data to estimate external forces and moments through factor graph optimization [7]. The estimated forces can then be incorporated into a model predictive control (MPC) framework to optimize footprint placement for disturbance rejection. Despite these advances, existing model-based approaches have two key limitations: (i) they are typically restricted to handling small perturbations (less than 50N), and (ii) they rely on pre-defined gaits, which constrain the robot to low-speed locomotion. These limitations significantly undermine the robot's ability to respond effectively to large, impulsive external forces. Barrier Lyapunov Functions (BLF) have been applied in domains such as autonomous driving to guarantee safety [10]. However, extending this approach to quadruped robots is non-trivial, as their highly nonlinear dynamics under dynamic locomotion make real-time implementation computationally demanding.

Reinforcement learning (RL) based methods, on the other hand, demonstrate stronger generalization and robustness to larger impulse disturbances. For example, Hartmann et al. proposed a multi-stage episodic training setup with reward shaping for robots to respond less aggressively to transient perturbations [11]. However, this approach is still not effective against large persistent forces. Inspired by biomechanics, Li et al. proposed a torque-based policy that directly outputs joint-level torques such that the quadruped robot can adapt to sudden disturbances acting on the legs and exhibits compliance to external forces in all directions [12]. However, the resulting fixed compliance prevents the robot from reliably following velocity commands under external pushes and doesn't incorporate adjustable compliance behavior. To address this limitation, Zhou et al. proposed to apply hierarchical reinforcement learning for active compliance control [13]. In this framework, a high-level RL planner modulates velocity commands according to external forces so that the robot can actively follow velocity targets while complying with external forces. Despite its advantages, the method has notable limitations: (i) the force estimation module is trained jointly with the low-level policy, which reduces the functional role of the high-level planner, and (ii) modifying compliance parameters requires retraining the high-level policy, limiting flexibility and efficiency. Concurrently with our work, Xu et al. proposed a RL framework that integrates a virtual mass-spring-damper model for reference generation and tracking [14]. This approach enables robust velocity compliance with adjustable compliance levels. However, its success rate decreases when external forces exceed 500N, highlighting the limitation of relying on a single policy to achieve both precise velocity tracking and high force tolerance. Our work, in comparison with existing methods, has several advantages as shown in Table I.

TABLE I

COMPARISON OF DIFFERENT METHODS (M: MODEL-BASED, L: LEARNING-BASED). ES: NO EXTRA SENSOR REQUIRED, VC: VELOCITY COMPLIANCE, AC: ADJUSTABLE COMPLIANCE LEVEL, LR: LARGE IMPULSE REJECTION.

Method (paradigm)	ES	VC	AC	LR
Kang et al. [7] (M)	✗	✗	✗	✗
Hartmann et al. [11] (L)	✓	✗	✗	✗
Zhou et al. [13] (L)	✓	✓	✗	✗
Xu et al. [14] (L)	✓	✓	✓	✗
SAC-Loco (L)	✓	✓	✓	✓

III. METHODS

A. Overview

The framework of the safe and adjustable compliant control is shown in Fig. 2. First, we use RL to train a teacher compliant policy π_{comply}^* , with adjustable compliance level. We distill π_{comply}^* into the student compliant policy π_{comply} , such that the policy can be deployed on the robot without using a force estimation module. Then, we collect rollouts from π_{comply} , identify failure cases and construct a dataset $\mathcal{D}_{\text{unsafe}}$ that contains unsafe states. Then, we train a teacher safe policy π_{safe}^* that is designed to recover from $s_{\text{unsafe}} \in \mathcal{D}_{\text{unsafe}}$ and sustain large impulses. After distilling into the student safe policy π_{safe} , we collect observation rollouts from π_{safe} and train a recoverability network V_{recover} that predicts if an observation o_t can be recovered by π_{safe} or not. During deployment, V_{recover} serves as a policy switching mechanism to switch from π_{comply} to π_{safe} using its value output.

B. Teacher Compliant Policy training

The force compliant policy's objective is to make the robot track a desired velocity, $\mathbf{v}^* = [v_x^*, v_y^*]$ computed by the velocity generator. The velocity generator receives a command, $\mathbf{c} = [v'_x, v'_y, \omega'_z, k]$, which contains the commanded linear velocity in robot's body frame of reference, the commanded angular velocity in z -axis and the compliance level parameter. The velocity generator observes the external force, $\mathbf{F} = [F_x, F_y, F_z]$, applied on the robot and computes the desired velocity as

$$v_x^* = v'_x + kF_x, \quad (1)$$

$$v_y^* = v'_y + kF_y. \quad (2)$$

The desired velocities generated, if followed by the robot, would enable the robot to achieve adjustable compliance behaviors under external forces. For the Unitree Go2 robot, we can obtain the Inertia Measurement Unit (IMU) information and joint level information. Therefore, the observable states of the robot is given by

$$\mathbf{x}_t = [\mathbf{g}_t, \omega_t, \mathbf{q}_t, \dot{\mathbf{q}}_t, \mathbf{a}_{t-1}, \mathbf{c}], \quad (3)$$

where $\mathbf{g}_t \in \mathbb{R}^3$ are the projected gravity, $\omega_t \in \mathbb{R}^3$ the body angular velocities, $\mathbf{q}_t, \dot{\mathbf{q}}_t \in \mathbb{R}^{12}$ are the joint angles and velocities, $\mathbf{a}_{t-1} \in \mathbb{R}^{12}$ the previous action, and $\mathbf{c} \in \mathbb{R}^4$ the command. We first train a teacher force compliant policy

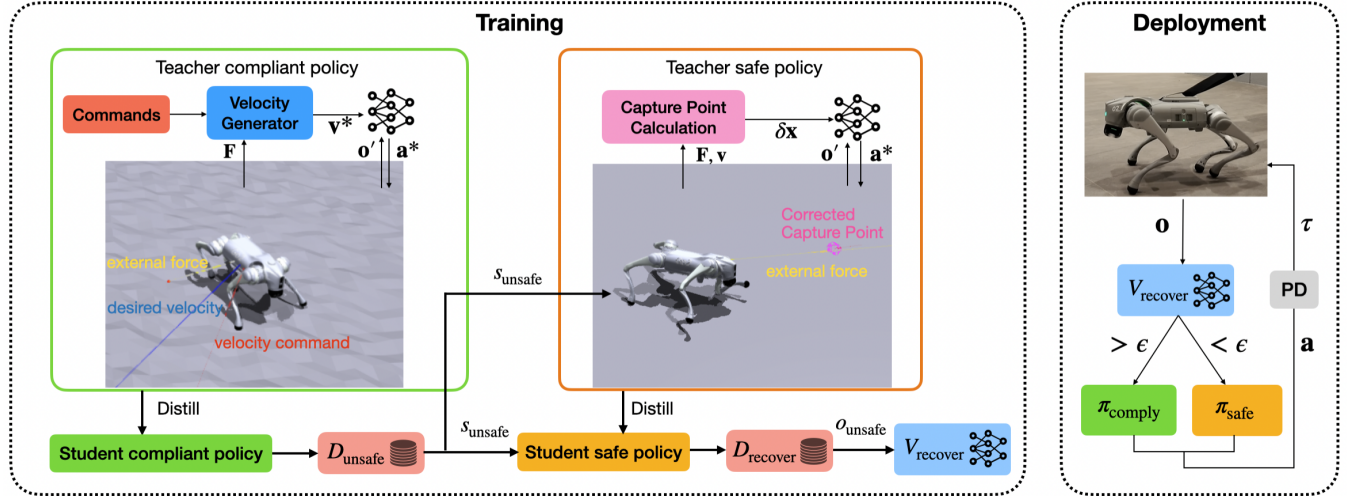


Fig. 2. Overview of SAC-Loco.

π_{comply}^* using additional privileged observations obtained in simulations

$$o'_t = [\mathbf{x}_t, \mathbf{Q}_t, \mathbf{v}_t, \mathbf{F}_t, \tau_t], \quad (4)$$

where $\mathbf{Q}_t \in \mathbb{R}^4$, $\mathbf{v}_t \in \mathbb{R}^3$, $\mathbf{F}_t \in \mathbb{R}^3$, and $\tau_t \in \mathbb{R}^3$ correspond to body orientation, body velocity, external force, and external torque, respectively. The reward functions consists of velocity tracking rewards that enable the robot to follow the desired velocity \mathbf{v}^* computed by the velocity generator. Regularization rewards are included to help robot maintain stable posture and smooth joint level actions. The detailed reward terms and corresponding weights are shown in Table II.

C. Teacher Safe policy training

The safe policy's objective is to help robot sustain large force impulses. We adopt the Corrected Capture Point (CCP) concept from [7]. Based on the linear inverted pendulum model (LIPM) [15], the CCP calculates a desired position offset for the robot to reach in order to restore balance

$$\delta_x = \sqrt{\frac{z_h}{g}} v_x + \frac{F_x z_h}{mg}, \quad (5)$$

$$\delta_y = \sqrt{\frac{z_h}{g}} v_y + \frac{F_y z_h}{mg}, \quad (6)$$

where z_h is the base height of the robot, m is the mass of the robot and g is the gravitational constant. For a quadruped robot, due to its physical structure, it can sustain a larger force in the longitudinal (x -axis) direction than in the lateral (y -axis) direction. Therefore, we further design a target yaw angle calculation

$$\psi^* = \begin{cases} \text{atan2}(F_y, F_x), & \text{if } F_x \geq 0 \\ \text{atan2}(F_y, F_x) + \pi, & \text{if } F_x < 0 \end{cases}, \quad (7)$$

such that the robot's x -axis aligns with the direction of the external force, thereby increasing its tolerance to larger disturbances. When the force is applied toward the robot's head, the robot turns to align its head with the force direction.

Conversely, when the force is applied toward the tail, the robot rotates to align its tail with the force direction. An visualization of the capture point and target yaw calculation is shown in Fig. 3. In order for the robot to move to the

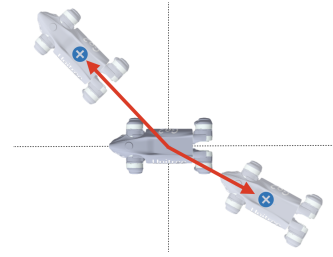


Fig. 3. Visualization of the calculated capture point and yaw angle when robot experience a force. Red arrow represents the push force vector. Blue marker represents the corrected capture point.

capture point as fast as possible, we use two-stages training. In the first stage, we train the robot move to any randomly sampled target position offset command $\delta\mathbf{x} = [\delta_x, \delta_y, \psi^*]$ that consists of the x, y position offset and a yaw angle target. In the second stage, we start exerting external forces on the robot and use the CCP calculation (5) - (7) results as the command. This policy takes the same observation as (4), with $\mathbf{c} = \delta\mathbf{x}$. The reward functions are designed to help robot achieve precise and fast positional reaching. Inspired by [16] and [4], we use reward shaping focusing on minimizing the position error of the robot. The detailed reward terms and their corresponding weight are shown in Table II.

D. Student policy distillation

After training the two teacher policies, we distill them into student policies π_{comply} and π_{safe} that can be deployed on the physical robot using only the observable states defined in (3). To compensate for the lack of privileged information, the student's policy receives as input a stacked observation history of length 20

$$o_t = [\mathbf{x}_{t-20}, \mathbf{x}_{t-19}, \dots, \mathbf{x}_{t-1}, \mathbf{x}_t]. \quad (8)$$

TABLE II

REWARD FUNCTIONS FOR π_{COMPLY}^* (MARKED †), π_{SAFE}^* (MARKED *),
SHARED REGULARIZATION TERMS (NO MARK), AND THEIR
CORRESPONDING WEIGHTS.

Name	Expression	Weight
Linear velocity tracking †	$\exp\left(-\frac{\ v_{xy}^* - v_{xy}\ ^2}{0.25}\right)$	1.0
Angular velocity tracking †	$\exp\left(-\frac{\ \omega_z' - \omega_z\ ^2}{0.25}\right)$	0.5
Position tracking soft *	$\frac{1}{1 + \ \delta x + \delta y\ ^2}$	20.0
Position tracking tight *	$\frac{1}{1 + \ \frac{\delta x + \delta y}{0.5}\ ^2}$	20.0
Yaw angle tracking *	$\frac{1}{1 + \ \frac{\psi - \psi^*}{0.5}\ ^2}$	20.0
Velocity direction *	$\max\left(0, \frac{v_x \delta_x}{\sqrt{\delta_x^2 + \delta_y^2}} + \frac{v_y \delta_y}{\sqrt{\delta_x^2 + \delta_y^2}}\right)$	40.0
Yaw rate direction *	$\dot{\psi} \cdot \text{sign}(\text{wrap}(\psi^* - \psi))$	20.0
Stand still *	$(\ v_{xy}\ < 0.5 \wedge \dot{\psi} < 0.1 \wedge h > 0.26) \cdot \mathbf{1}_{\text{reached}}$	20.0
Base height	$(h_z - 0.25)^2$	-0.5
Angular velocity penalty	$\ \omega_{xy}\ ^2$	-0.05
Torques	$\ \boldsymbol{\tau}\ _2^2$	-0.0005
Joint velocities	$\ \dot{\mathbf{q}}\ _2^2$	-0.0001
Joint accelerations	$\left\ \frac{\dot{\mathbf{q}}_{t-1} - \dot{\mathbf{q}}_t}{dt}\right\ ^2$	-2.5e-7
Action rate	$\left\ \frac{\dot{\mathbf{a}}_{t-1} - \dot{\mathbf{a}}_t}{dt}\right\ ^2$	-0.01
Joint angle limit	$\sum_{i=1}^{12} (q_i - 0.9 \cdot q_{i,\text{lim}})$	-10.0
Joint velocity limit	$\sum_{i=1}^{12} (\dot{q}_i - 0.9 \cdot \dot{q}_{i,\text{lim}})$	-5.0
Joint torque limit	$\sum_{i=1}^{12} (\tau_i - 0.85 \cdot \tau_{i,\text{lim}})$	-5.0
Feet air time	$\sum t_{\text{feet}} \text{ if } F_{\text{feet}} < 0$	2.0
Collision	$F_{\text{base,thigh,calf}} > 0$	-10.0

To achieve efficient training and a balance between exploration and exploitation, we use the PPO distillation method in [17]. We compute the mean squared error (MSE) loss between the teacher's actions and the student's actions

$$\mathcal{L}_{\text{distillation}} = \|\pi^*(o'_t) - \pi(o_t)\|_2^2, \quad (9)$$

and the total loss for PPO becomes

$$\mathcal{L}_{\text{total}} = \alpha \mathcal{L}_{\text{distillation}} + \beta \mathcal{L}_{\text{PPO}}. \quad (10)$$

To facilitate early stage exploration in the correct direction, we also added two additional reward terms inspired by [18] to guide the student policy's actions to stay close to the teacher policy's actions

$$r_{\text{action}} = \exp\left(-\frac{\|a_t^* - a_t\|^2}{0.5}\right), \quad (11)$$

$$r_{\text{direction}} = e^{\frac{a_t \cdot a_t^*}{\|a_t\| \|a_t^*\|}}, \quad (12)$$

where a_t^* and a_t are the teacher's and student's actions at timestep t . To increase sample efficiency, we adopt asymmetric PPO, where the critic additionally observes the privileged observation o'_t in (4).

E. Recoverability Network

In order to switch from π_{comply} to π_{safe} before the robot falls. We train a recoverability network V_{recover} that monitors the robot's observations at real time. Unlike prior policy

switching approaches (e.g. [4], [19]), which either condition on a single policy or are trained to be fixed, our network leverages information from both policies and can be used more flexible. We first collect rollouts from π_{comply} in simulation under random commands and external perturbations. A failure is defined as the robot's base make contact with the ground. When a failure occurs, we store the preceding 100 states to the unsafe dataset $\mathcal{D}_{\text{unsafe}}$. Each state is represented as

$$s_t = [h_{zt}, \mathbf{v}_t, \omega_t, \mathbf{q}_t, \dot{\mathbf{q}}_t, \mathbf{F}_t, \tau_t], \quad (13)$$

which consists of robot's base and joint physical states as well as the external force and torque that it is experiencing. The dataset $\mathcal{D}_{\text{unsafe}}$ serves two purposes. First, during training of π_{safe} , we sample s_{unsafe} from $\mathcal{D}_{\text{unsafe}}$ as robot's state initialization, allowing the policy to practice recovery from potentially dangerous conditions. Second, after π_{safe} is trained, we sample o_{unsafe} and s_{unsafe} from $\mathcal{D}_{\text{unsafe}}$ and evaluate whether π_{safe} can successfully recover robot. The success and failure labels associate with each o_{unsafe} is added to the recover dataset $\mathcal{D}_{\text{recover}}$. Finally, V_{recover} is trained on $\mathcal{D}_{\text{recover}}$ using gradient descent. The data collection and training process for recoverability network is shown in Algotirhm 1. During deployment, the output of $V_{\text{recover}}(o_t) \in [0, 1]$ will be compared to a threshold ϵ . If V_{recover} falls below the ϵ , π_{safe} will be activated to control the robot.

Algorithm 1 Recoverability Network Training

```

1: Init  $\mathcal{D}_{\text{unsafe}} \leftarrow \emptyset$ 
2: for episode = 1 to  $N$  do
3:   for each step  $t = 0, 1, \dots, T$  do
4:      $\{o_{t-k}\}_{k=0}^{100}, \{s_{t-k}\}_{k=0}^{100} \sim p(\cdot | \pi_{\text{comply}}(o_t))$ 
5:     if Failure then
6:        $\mathcal{D}_{\text{unsafe}} \leftarrow \mathcal{D}_{\text{unsafe}} \cup \{o_{t-k}\}_{k=0}^{100}, \{s_{t-k}\}_{k=0}^{100}$ 
7:     end if
8:   end for
9: end for
10: Init  $\mathcal{D}_{\text{recover}} \leftarrow \emptyset, V_{\text{recover}}^{\theta}$  params  $\theta$ 
11: for episode = 1 to  $N$  do
12:   Sample  $o_{\text{unsafe}}, s_{\text{unsafe}} \sim \mathcal{D}_{\text{unsafe}}$ 
13:   Initialize Environment with  $s_{\text{unsafe}}$ 
14:   for each step  $t = 0, 1, \dots, T$  do
15:     Success, Failure  $\sim p(\cdot | \pi_{\text{safe}}(o_t))$ 
16:     if Success then
17:        $\mathcal{D}_{\text{recover}} \leftarrow \mathcal{D}_{\text{recover}} \cup \{(o_{\text{unsafe}}, 1)\}$ 
18:     else
19:        $\mathcal{D}_{\text{recover}} \leftarrow \mathcal{D}_{\text{recover}} \cup \{(o_{\text{unsafe}}, 0)\}$ 
20:     end if
21:   end for
22:   Sample batch  $(o_{\text{unsafe}}, y) \sim \mathcal{D}_{\text{recover}}$ 
23:   Compute loss  $\ell = \ell(V_{\text{recover}}(o_{\text{unsafe}}; \theta), y)$ 
24:   Update  $\theta \leftarrow \theta - \eta \nabla_{\theta} \ell$ 
25: end for

```

F. Training details

We train all policies using the Isaac Gym simulator [20] using 4096 environments in parallel with the PPO algo-

TABLE III
DOMAIN RANDOMIZATION PARAMETER

Term	Value
Dynamics	Robot mass $\mathcal{U}(12.75, 17.25)$ kg
	Friction coefficient $\mathcal{U}(-0.5, 2.0)$
	Joint K_p gain $\mathcal{U}(19, 21)$
	Joint K_d gain $\mathcal{U}(0.48, 0.52)$
	ERFI-50 [22] $0.78\text{Nm} \times \text{Curriculum}$
	Joint bias $\mathcal{U}(-0.08, 0.08)$
Sensor noises	Base angular velocity $\mathcal{U}(-0.25, 0.25)$ rad/s
	Gravity vector $\mathcal{U}(-0.1, 0.1)$
	Joint positions $\mathcal{U}(-0.015, 0.015)$ rad
	Joint velocities $\mathcal{U}(-1.5, 1.5)$ rad/s
Disturbances	$F_{x,y}$ $\mathcal{U}(-700, 700)$ N
	F_z $\mathcal{U}(-50, 50)$ N
	$\tau_{x,y}$ $\mathcal{U}(-50, 50)$ Nm
	τ_z $\mathcal{U}(-20, 20)$ Nm
Commands	Impact time length $\mathcal{U}(0.5, 3)$ sec
	k $\mathcal{U}(0.0, 0.02)$
	v'_x $\mathcal{U}(-2.5, 2.5)$ m/s
	v'_y $\mathcal{U}(-2, 2)$ m/s
	ω'_z $\mathcal{U}(-1.5, 1.5)$ rad/s

rithm [21]. We applied curriculum learning that gradually increases command velocities, external forces and torque magnitude, and terrain levels. Domain randomization and noise are applied to reduce the sim to real gap. The domain randomization details are shown in Table III.

IV. SIMULATION RESULTS

A. Compliant policy performance

π_{comply} is expected to make the robot track \mathbf{v}^* computed by the velocity generator. To demonstrate the effectiveness of π_{comply} in achieving adjustable compliance, we set a velocity command $v'_x = 0.5\text{m/s}$, $v'_y = 0\text{m/s}$, $\omega'_z = 0\text{rad/s}$. A sinusoid external force $F_y = 100 \cdot \sin(0.5t)$ is applied. As shown in Fig. 4, with $k = 0$, the robot resists the external force and tracks the command velocity. When k is increased to 0.01 and 0.02, v_y changes with F_y in the same direction and the magnitude increases with k . However, it can be seen that larger k undermines velocity tracking of v'_x although no F_x is applied.

Ablation study is done by performing three other trainings:

- 1) Training π_{comply} directly without using a teacher policy (π_{comply} w/o T).
- 2) Training π_{comply} without the velocity generator (π_{comply} w/o \mathbf{v}^*).
- 3) Training π_{comply} directly without both the velocity generator and the teacher policy (π_{comply} w/o T & \mathbf{v}^*).

We observe that training π_{comply} w/o T fails to produce a valid policy: the robot collapses to the ground without moving. This is expected since without the teacher policy's guidance, the student cannot track the continuously varying but unobservable \mathbf{v}^* and gets stuck in a local minimum. We evaluate the compliance performance of each policy by calculating the episode average error between robot's velocity \mathbf{v} and \mathbf{v}^*

$$e_x = \frac{1}{T} \sum_{t=1}^T |v_{xt} - v_{xt}^*|, e_y = \frac{1}{T} \sum_{t=1}^T |v_{yt} - v_{yt}^*|, \quad (14)$$

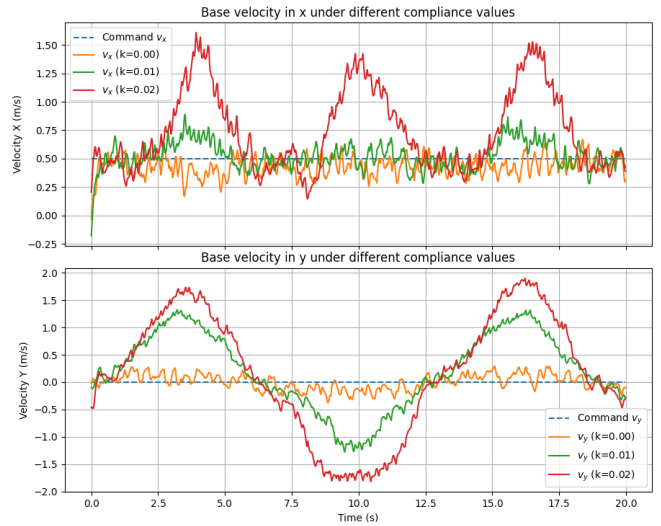


Fig. 4. Velocity tracking performance of π_{comply} with different compliance level parameter k under an external sinusoid force in y -axis.

where T is the episode length. We run 4096 environments in parallel for 10 episodes with the same domain randomization in Table III. The average error and failure rate is summarized in Table IV. π_{comply} w/o \mathbf{v}^* is essentially π_{comply} with $k = 0$. Therefore, it has a worse compliance behavior. However, the teacher policy helps it to learn privileged observations such as external force, making its failure rate lower than π_{comply} w/o T & \mathbf{v}^* . π_{comply} w/o T & \mathbf{v}^* , which has no access to privileged observations, suffers higher failure rate and worse compliance.

TABLE IV
ABLATION STUDY FOR COMPLIANCE AND SAFETY PERFORMANCE
UNDER DIFFERENT RANGE OF EXTERNAL FORCE. (MEAN \pm STD DEV)

	\bar{e}_x (m/s)	\bar{e}_y (m/s)	Failure rate (%)
$F_{xy} = 0 \sim 200\text{N}$			
π_{comply}	0.181 ± 0.001	0.161 ± 0.001	0
π_{comply} w/o \mathbf{v}^*	0.334 ± 0.038	0.290 ± 0.027	0.16 ± 0.01
π_{comply} w/o T & \mathbf{v}^*	0.685 ± 0.033	0.497 ± 0.028	1.47 ± 0.50
$F_{xy} = 200 \sim 400\text{N}$			
π_{comply}	0.252 ± 0.001	0.203 ± 0.001	0.09 ± 0.04
π_{comply} w/o \mathbf{v}^*	0.487 ± 0.004	0.393 ± 0.002	0.29 ± 0.05
π_{comply} w/o T & \mathbf{v}^*	0.729 ± 0.018	0.557 ± 0.012	49.81 ± 2.47
$F_{xy} = 400 \sim 600\text{N}$			
π_{comply}	0.401 ± 0.002	0.276 ± 0.001	6.25 ± 0.09
π_{comply} w/o \mathbf{v}^*	0.513 ± 0.009	0.394 ± 0.006	15.58 ± 0.14
π_{comply} w/o T & \mathbf{v}^*	0.858 ± 0.013	0.639 ± 0.007	99.9 ± 0.03

B. Safe policy performance

We tested π_{safe} and V_{recover} with larger force impulses. As shown in Fig. 5, when small forces are applied (green region), π_{comply} is activated. When large forces are applied (red region), V_{recover} falls under $\epsilon = 0.9$ and π_{safe} is activated to bring the robot back to a safe state, and π_{comply} is then switched back.

To evaluate the effect of V_{recover} and the tunable parameter ϵ , we collect rollouts from 4096 environments in parallel for 10 episodes. In each test, a horizontal force F_{xy} of fixed

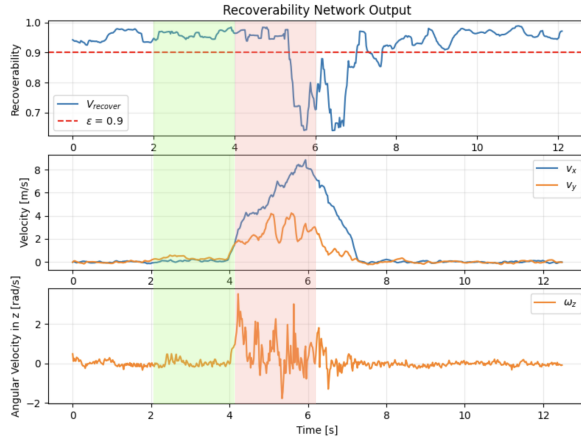


Fig. 5. Recoverability network output and the robot's velocities when the robot is pushed with two sets of forces: $F_x = 50\text{N}$, $F_y = 100\text{N}$ (green). $F_x = F_y = 600\text{N}$ (red). π_{safe} is activated when recoverability network output fall below $\epsilon = 0.9$.

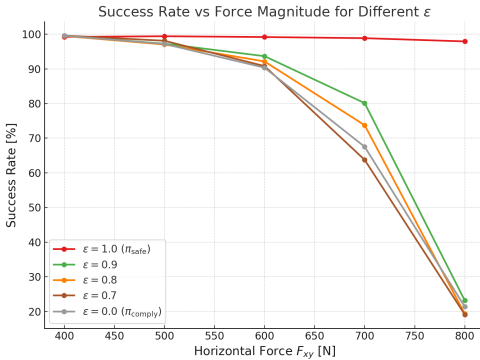


Fig. 6. Success rate under different magnitude of horizontal force with different recoverability network threshold ϵ for policy switching.

magnitude but random in xy direction is applied. Each push lasts between 1 - 2 seconds. We calculate the success rate of different ϵ . The result is shown in Fig. 6. When $\epsilon = 1.0$ (only using π_{safe}), the success rate is very good even with 800N of F_{xy} . When $\epsilon = 0.0$ (only using π_{comply}), the success rate drops below 90% when $F_{xy} > 600\text{N}$. With $\epsilon > 0.7$, π_{safe} helps increasing the success rate.

V. HARDWARE DEPLOYMENT

We deployed SAC-Loco onto the Unitree Go2 quadruped robot. The policy runs at 50 Hz on the Unitree Go2 Jetson Orin NX. We performed three experiments to verify our policy's effectiveness.

First, we tied the robot to another robot (leader). We control the leader to pull the robot in the lateral direction and in the forward direction. We compare our method with Model Predictive Control (MPC) and vanilla reinforcement learning control (Base-RL). As shown in Fig. 8 (a) - (f), the robot with Base-RL (a)(d) tends to lose balance and tilt toward the pulling force. MPC (b)(e) is compliant in the forward direction and can follow the leader robot with better stability, but is not compliant in the lateral direction, refusing to move when pulled laterally. In contrast, ours (c)(f) can follow by the leader in all directions with stable pose.

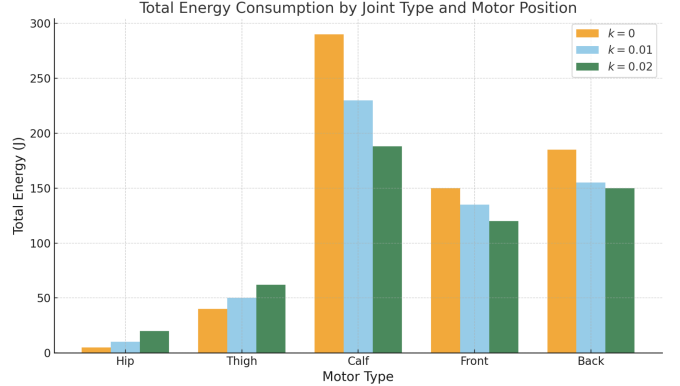


Fig. 7. Motor energy consumption when robot pulling the chair with different compliance level for different motor type and positions.

Second, we tied the robot to an office chair with a person in the seat. The robot is given a constant velocity command of $v'_x = 0.6\text{m/s}$. The total weight of chair and person is around 70 kg. We tested three different compliance parameters for this task. As shown in Fig. 8 (g), the robot's velocity changes with different compliance level parameters. With $k = 0$, the robot resists the counter force and pulls the chair with larger velocity. With $k = 0.02$, the robot becomes more affected by the counter force and travels at a lower velocity. We calculated the energy consumed by each motor during the process $E_i = \int_{t_0}^{t_f} \tau_i(t) \dot{q}_i(t) dt$. We group motor energy consumption by joint type and position, as shown in Fig. 7. Overall, total energy consumption decreases as compliance increases. Furthermore, with higher compliance levels, the calf motors exhibit reduced energy consumption, while the hip and thigh motors show increased energy consumption, reflecting a redistribution of effort across the joints. In addition, the rear motors consume more energy than the front motors, since the robot is pulling an external load from its behind.

Third, we tested large impulse on the robot by manually dragging the robot suddenly and tries to make it fall over. As shown in Fig. 8 (h), π_{safe} effectively prevents the robot from falling over.

VI. CONCLUSION

This paper presented SAC-Loco, a novel switched-policy controller for quadruped robots to achieve adjustable compliant velocity tracking under external disturbances, a recoverability network predicts potential failures and a safe policy enhances robustness against large impulses. Together, these components form a unified solution for smooth compliance and reliable failure prevention in dynamic environments.

Extensive simulation and hardware experiments validate the effectiveness and practicality of SAC-Loco. Compared with previous work, our approach allows for adjustable compliance levels and safe policy switching, broadening the range of compliant behaviors a quadruped can exhibit under external forces. These adjustable parameters open avenues for future research. In particular, further work can explore adaptive adjustment of compliance and switching parameters in response to varying environments and tasks.

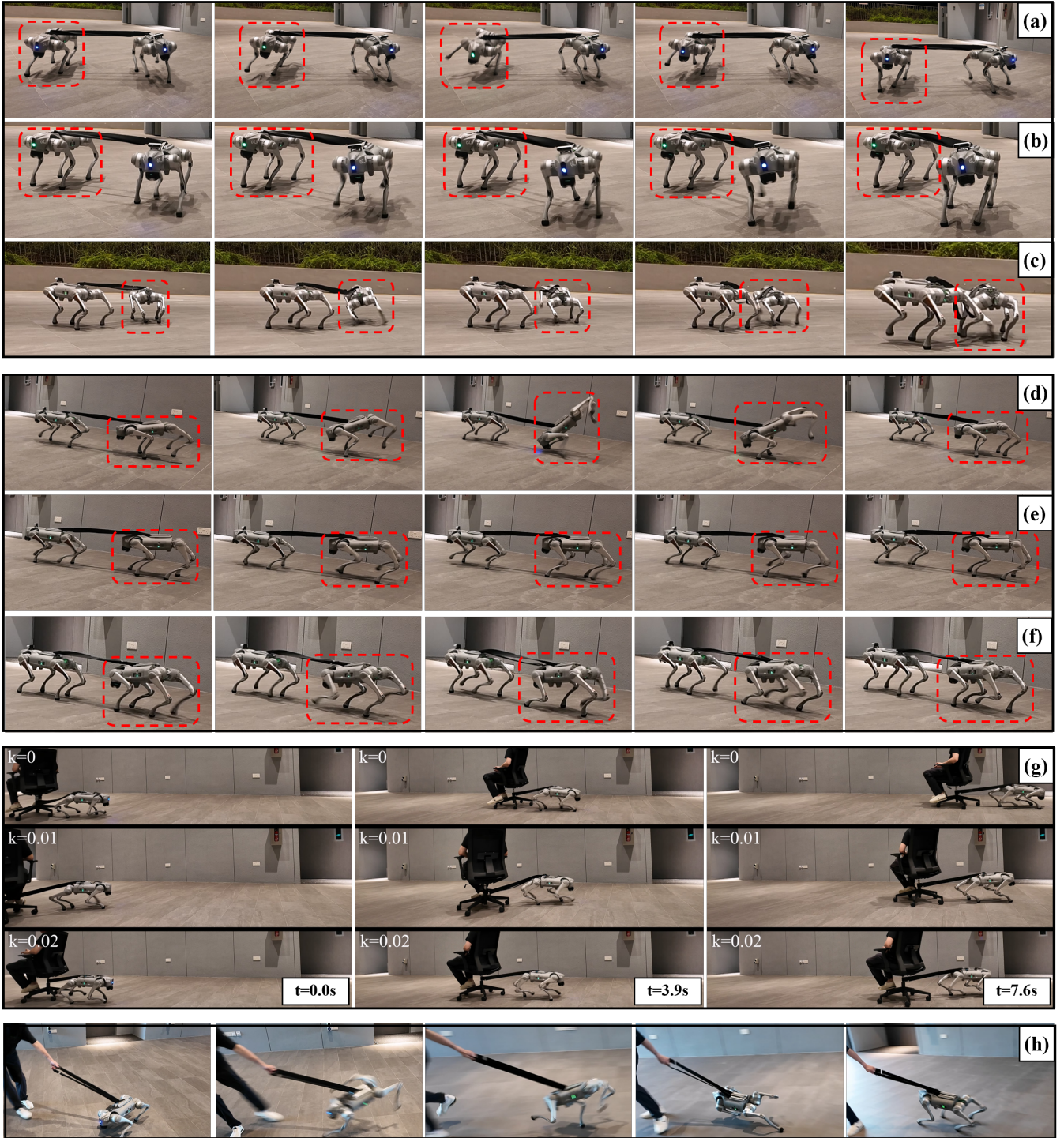


Fig. 8. Hardware experiments. In the **Dragging Experiment**, one quadruped robot is connected to another with a rope. The front robot pulls the rear robot, with the pulling force applied either laterally shown in (a)(b)(c) or in the forward direction shown in (d)(e)(f). The rear robot (highlighted by the red box) is controlled by three different controllers: (a)(d) **Base-RL**, (b)(e) **MPC**, and (c)(f) **Ours**.

In the **Towing Experiment**, a quadruped robot is connected to an office chair with a seated person, and the robot is set to a constant velocity command of $v_x' = 0.6m/s$ and pulls the chair forward shown in (g). By adjusting different values of k , the pulling speed is varied. Subfigure (g) shows three snapshots at 0 seconds, 3.9 seconds, and 7.6 seconds, respectively.

In the **Violent Dragging Experiment**, we suddenly drag the robot violently. The robot reponses by jumping toward the force and restores balance.

REFERENCES

- [1] X. Cheng, K. Shi, A. Agarwal, and D. Pathak, “Extreme parkour with legged robots,” in *Proceedings of the 2024 IEEE International Conference on Robotics and Automation (ICRA)*. Yokohama, Japan: IEEE, 2024, pp. 11 443–11 450.
- [2] Y. Ji, G. B. Margolis, and P. Agrawal, “Dribblebot: Dynamic legged manipulation in the wild,” in *Proceedings of the 2023 IEEE International Conference on Robotics and Automation (ICRA)*. IEEE, 2023.
- [3] P. Arm, M. Mittal, H. Kolvenbach, and M. Hutter, “Pedipulate: Enabling manipulation skills using a quadruped robot’s leg,” in *Proceedings of the 2024 IEEE International Conference on Robotics and Automation (ICRA)*, Yokohama, Japan, 2024, pp. 5717–5723.
- [4] T. He, B. Lan, R. Hasani, and D. Rus, “Agile but safe: Learning collision-free high-speed legged locomotion,” *arXiv preprint arXiv:2401.17583*, 2024.
- [5] H. Kim, H. Oh, J. Park, Y. Kim, D. Youm, M. Jung, M. Lee, and J. Hwangbo, “High-speed control and navigation for quadrupedal robots on complex and discrete terrain,” 2025.
- [6] C. Zhang, J. Jin, J. Frey, N. Rudin, M. Mattamala, C. Cadena, and M. Hutter, “Resilient legged local navigation: Learning to traverse with compromised perception end-to-end,” in *2024 IEEE International Conference on Robotics and Automation (ICRA)*, Yokohama, Japan, 2024, pp. 34–41.
- [7] J. Kang, H.-B. Kim, B.-I. Ham, and K.-S. Kim, “External force adaptive control in legged robots through footstep optimization and disturbance feedback,” *IEEE Access*, vol. 12, pp. 157 531–157 539, 2024.
- [8] Z. Xiao, J. Huang, Q. Gong, D. Fan, Z. Liu, and F. Gao, “Pa-loco: Learning perturbation-adaptive locomotion for quadruped robots,” in *2024 IEEE/RSJ International Conference on Intelligent Robots and Systems (IROS)*. IEEE, 2024.
- [9] N. Khandelwal, A. Manu, S. S. Gupta, M. Kothari, P. Krishnamurthy, and F. Khorrami, “Compliant control of quadruped robots for assistive load carrying,” 2025.
- [10] Y. Zhang *et al.*, “Barrier lyapunov function-based safe reinforcement learning for autonomous vehicles with optimized backstepping,” *IEEE Transactions on Neural Networks and Learning Systems*, vol. 35, no. 2, pp. 2066–2080, Feb. 2024.
- [11] A. Hartmann, D. Kang, F. Zargarbashi, M. Zamora, and S. Coros, “Deep compliant control for legged robots,” in *Proceedings of the 2024 IEEE International Conference on Robotics and Automation (ICRA)*, Yokohama, Japan, 2024, pp. 11 421–11 427.
- [12] P. Li, H. Li, G. Sun, J. Cheng, X. Yang, G. Bellegarda, M. Shafiee, Y. Cao, A. Ijspeert, and G. Sartoretti, “Sata: Safe and adaptive torque-based locomotion policies inspired by animal learning,” 2025.
- [13] X. Zhou, X. Zhang, and Q. Zhang, “Hac-loco: Learning hierarchical active compliance control for quadruped locomotion under continuous external disturbances,” 2025.
- [14] B. Xu, H. Weng, Q. Lu, Y. Gao, and H. Xu, “Facet: Force-adaptive control via impedance reference tracking for legged robots,” 2025.
- [15] J. Pratt, J. Carff, S. Drakunov, and A. Goswami, “Capture point: A step toward humanoid push recovery,” in *2006 6th IEEE-RAS International Conference on Humanoid Robots*, Genova, Italy, 2006, pp. 200–207.
- [16] J. Jin, C. Zhang, J. Frey, N. Rudin, M. Mattamala, C. Cadena, and M. Hutter, “Resilient legged local navigation: Learning to traverse with compromised perception end-to-end,” 2023.
- [17] Q. Zhang, G. Han, J. Sun, W. Zhao, C. Sun, J. Cao, J. Wang, Y. Guo, and R. Xu, “Distillation-ppo: A novel two-stage reinforcement learning framework for humanoid robot perceptive locomotion,” 2025.
- [18] T. Xu, Y. Cheng, P. Shen, and L. Zhao, “Acl: Action learner for fault-tolerant quadruped locomotion control,” 2025.
- [19] D. Jain, A. Iscen, and K. Caluwaerts, “Hierarchical reinforcement learning for quadruped locomotion,” 2019.
- [20] V. Makoviychuk, L. Wawrzyniak, Y. Guo, M. Lu, K. Storey, M. Macklin, D. Hoeller, N. Rudin, A. Allshire, A. Handa, and G. State, “Isaac gym: High performance gpu-based physics simulation for robot learning,” 2021.
- [21] J. Schulman, F. Wolski, P. Dhariwal, A. Radford, and O. Klimov, “Proximal policy optimization algorithms,” 2017.
- [22] L. Campanaro, S. Gangapurwala, W. Merkt, and I. Havoutis, “Learning and deploying robust locomotion policies with minimal dynamics randomization,” 2023.